Available online at www.sciencedirect.com

ScienceDirect

Advances in Space Research 54 (2014) 82–91

ADVANCES IN SPACE RESEARCH (a COSPAR publication)

www.elsevier.com/locate/asr

Development status of AEOLDOS – A deorbit module for small satellites

Patrick Harkness [a,*], Malcolm McRobb [a], Paul Lützkendorf [b], Ross Milligan [a], Andrew Feeney [a], Craig Clark [c]

[a] School of Engineering, University of Glasgow, Glasgow, UK
[b] Technische Universität München, Munich, Germany
[c] Clyde Space Ltd, Glasgow, UK

Received 28 June 2013; received in revised form 21 February 2014; accepted 23 March 2014
Available online 3 April 2014

Abstract

A prototype CubeSat module to deploy a gossamer aerobrake, using strain stored in tape-springs, at end-of-life is described. A novel hub geometry to reduce bending shock at end-of-deployment while simultaneously permitting radial, as opposed to tangential, deployment is proposed. The rpm of the hub is measured under various deployment conditions to verify that the system offers highly-repeatable performance, while high-speed photography is used to characterise the behaviour of the tape-spring during unspooling and contrast it to the behaviour of a traditional tangential-deployment system. Secondly the folding pattern of the membrane, which takes advantage of the symmetrical deployment offered by the petal hub, is developed and the unfolding mechanism is verified by numerical and experimental analysis. Finally, the release of the stored strain is considered and a novel burn-though device is designed and prototyped to meet this requirement.

Keywords: Petal-hub; Tape-spring; SMA; Aerobrake; CubeSat; Deorbit

1. Introduction

The risks associated with the build-up of orbital debris in Low Earth Orbit (LEO) are severe, and the development of the Inter-Agency Space Debris Coordination Committee reflects the growing international awareness of the problem over recent decades. Some form of end-of-life disposal is a cornerstone of almost all mitigation strategies, and deployable structures are often cited as a mechanism by which solar radiation pressure (Lücking et al., 2011), aerodynamic drag (Roberts and Harkness, 2007) or both (Ceriotti et al., 2013) can be used to provide the required de-orbit force. These methodologies, which have the advantage of not requiring fluid inflatants or rigidizing membranes (Freeland, 1998), are particularly attractive because they do not necessarily depend on the end-of-life spacecraft executing a burn (Roberts, 2004) or deploying a tether (Pardini et al., 2009), both of which often require a significant retained AOCS capability. Robustness is therefore a key advantage of these passive disposal strategies.

However, deploying a gossamer structure at end-of-life is not a simple matter either. The host spacecraft may have very limited remaining power and it will have been exposed to the space environment for a long period of time. Stored-strain systems, whereby the energy required for deployment is inherent in the stowed structure, are therefore attractive solutions provided that tribological issues are addressed.

Stored-strain systems of around 3U have flight heritage (Johnson et al., 2011) and further similarly-sized missions

* Corresponding author.
E-mail address: patrick.harkness@glasgow.ac.uk (P. Harkness).

http://dx.doi.org/10.1016/j.asr.2014.03.022
0273-1177/

are proposed (Lappas et al., 2011), where U is a standard CubeSat unit – 10 cm × 10 cm × 10 cm. However these devices are too large, by almost an order of magnitude, to provide a modular deorbit capability for most low cost CubeSat missions and, in general, larger aerobrakes tend to be more strongly associated with larger spacecraft (Kuwahara et al., 2011). Given that some CubeSat missions have an effective ceiling of approximately 650 km to ensure decay within the recommended timeframes set out IADC Space Debris Mitigation Guidelines (Lee, 2006) the provision of a small deployable aerobrake structure, compatible with leading CubeSat architectures, is a particularly attractive mechanism by which the ballistic coefficient of a small satellite could be reduced to speed final re-entry (King-Hele, 1987). The AEOLDOS (Aerodynamic End Of Life DeOrbit System) module is proposed to meet this need.

2. New concepts

Spooled tape-springs are commonly proposed as a deployment mechanism for gossamer membranes, often with several tangential tape-springs sharing a common hub. However, this approach leads to asymmetric membranes (see Fig. 1) which necessitate complicated folding patterns such as those proposed by Banik and Murphey (2007), and can place net transverse loads on the booms during deployment. Secondly, the mechanical shock at end-of-deployment can result in a peeling action (see Fig. 2) at the roots of the tape-springs.

2.1. Enabling concept #1: the petal-hub and associated technologies

The petal-hub system is proposed whereby final deployment is completely radial, peeling of the tape-springs is prevented, and the folding pattern is regularised. Also, considering the long dormancy end-of-life systems may experience, premature exposure of the aerobrake membrane to UV and atomic oxygen must be considered and protective doors are thus desirable. Complex door systems have been proposed elsewhere (Shmuel et al., 2012), but the sail-casting doors proposed for AEOLDOS, and enabled by the radial deployment, effectively combine deployment and sail extraction into a single passive event.

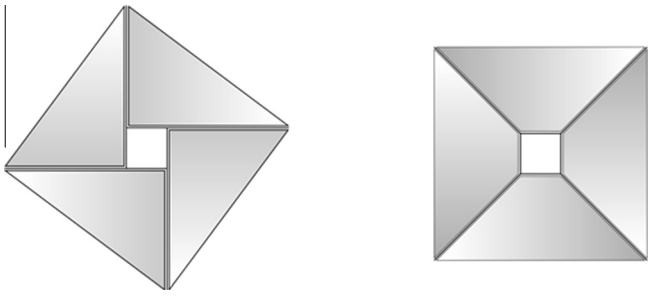

Fig. 1. Tangential deployment of the booms (left) leads to asymmetric sails and a more complex folding pattern than radial deployment (right).

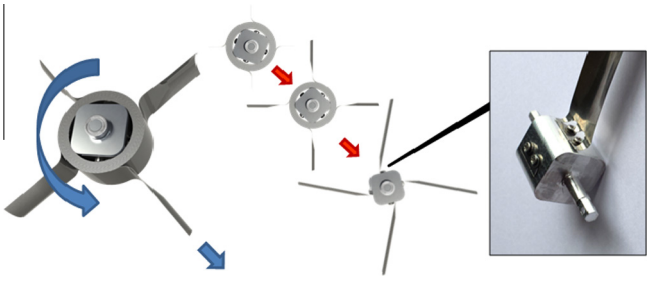

Fig. 2. This traditional hub rotates anticlockwise, deploying tangential booms with the support of guide bearings (not shown). However, at the end of the deployment, the rotational momentum of the hub applies a very considerable peeling load to the boom roots. This can cause failure at the points indicated on the right, and permanent deformation is visible from the very first deployment.

2.1.1. Membrane-free deployment tests

Fig. 2 illustrates the asymmetry and potential for fracture associated with tangential deployments. Fig. 3, however, illustrates how the petal-hub allows the booms to deploy and settle radially about the hub and, secondly, prevents excessive bending stresses near the connection point regardless of any transient post-deployment oscillations of the hub.

The operation of the petal-hub may be best understood through the series of drawings in Fig. 4. These illustrate the distribution of the tape-spring and movement of the doors as deployment proceeds following initial release of the hub, and further show the guide bearings that are used to prevent spool expansion and guide the booms away from the device. They also show the chambers that are used to stow the membrane, but omit the folded membrane for clarity.

The tape-springs have curved cross-sections, with the curvature all but disappearing when they are deflected onto a spool. The winding can place the natural curvature either concave or convex to the spool, with larger moments being required to force conformity in the convex-to-spool

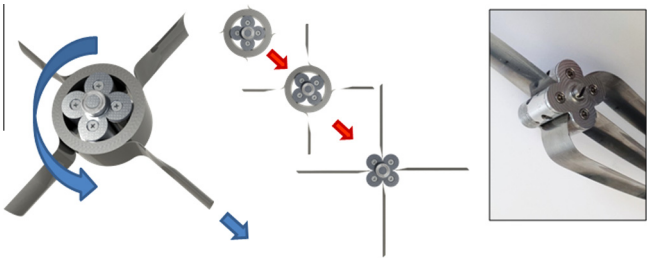

Fig. 3. This petal-hub rotates anticlockwise, deploying booms with the support of guide bearings (not shown). The booms adopt a radial shape at the end of the deployment process. Each petal prevents excessive bending of the booms where they attach to the hub, regardless of post-deployment behaviour, making failure much less likely (right). This constrained problem, with a known radius of curvature, allows the stress in the beam to be evaluated by Euler–Bernoulli beam theory if desired.

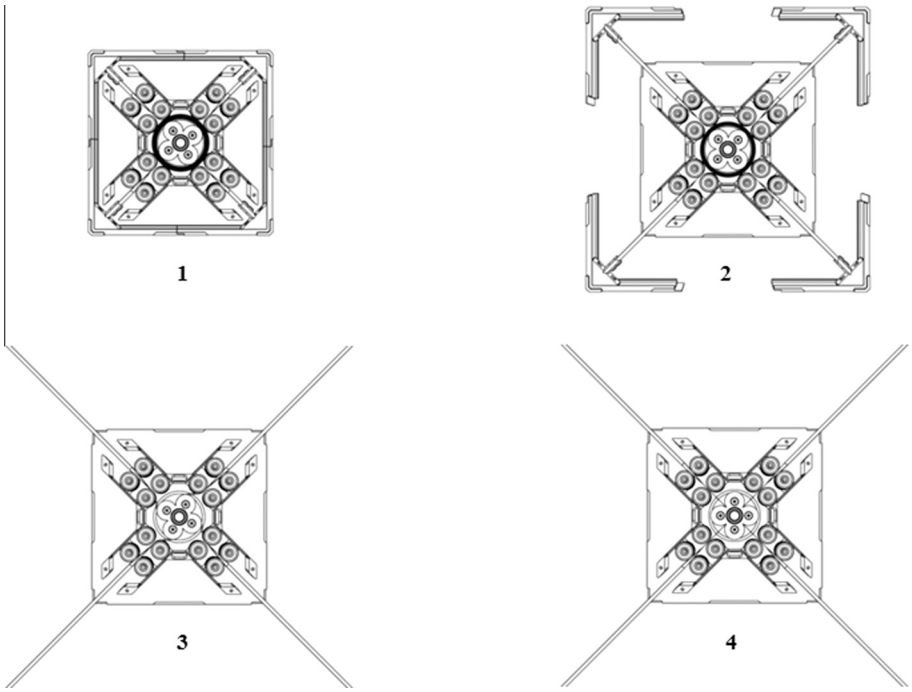

Fig. 4. A full deployment of an AEOLDOS device. The petal-hub prevents buckling at end-of-deployment and permits the booms to adopt a perfectly radial layout. The guide bearings and the chambers that accommodate the aerobrake membrane are now shown.

direction (Seffen and Pellegrino, 1999). This approach stores more energy and is preferred for the operation of the AEOLDOS device, although larger circumferential forces are required to retain the spool. This may be associated with an observed tendency to for these convex-to-spool systems to bulge out, or 'bloom' in the terminology of Jeon and Murphey (2011), between the guides during deployment. Nonetheless, this can be controlled by managing the guide separation and therefore, despite this difficulty, all subsequent results use the convex-to-spool technique.

To characterise the performance of the hubs an AEOLDOS module is equipped with a traditional and petal-type hub in turn, each of which has four coating-free tape-springs wound in the convex-to-spool manner. When the hubs are released by the action of a solenoid, a rate sensor acquires rpm histories while a high-speed camera obtains video footage. Typical results for boom lengths of 500 mm, 708 mm and 867 mm appear in Fig. 5 below, with the boom lengths being consistent with deployed aerobrake areas of 0.5 m^2, 1 m^2 and 1.5 m^2, respectively.

Fig. 5 illustrates that the petal-hub has limited influence on the early deployment characteristics, with both devices spinning up to around 3000 rpm in around 0.1 s, after which the power released by the booms stabilises to maintain the deployment rate. However, at the end of the deployment, the hub geometry has a marked effect. Both the traditional and petal-hubs have a final 'snap' of acceleration, but the petal-hub then permits the motion to damp out over multiple smooth oscillations as opposed to a few chaotic vibrations in the traditional hub.

It should be noted that the booms used with the traditional hub often failed, although not in any case presented

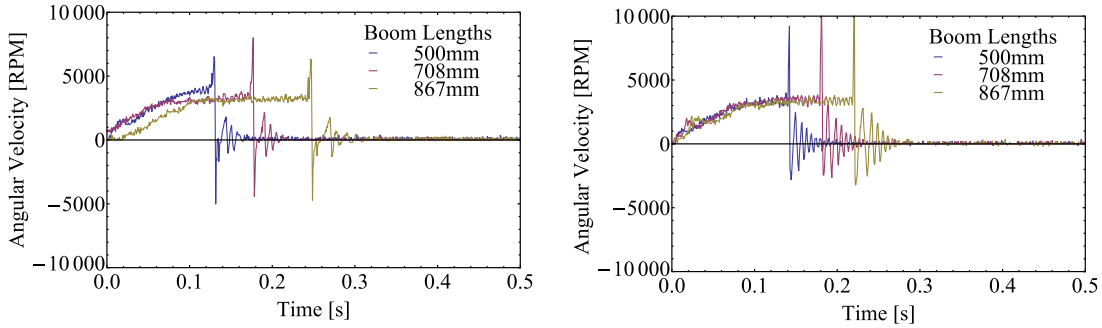

Fig. 5. The behaviour of a traditional hub (left) and a petal-hub (right), with boom lengths of 500 mm, 708 mm and 867 mm.

in Fig. 5, whereas those used with the petal hub did not fail in over twenty deployments.

2.1.2. Deployment tests with membranes

The AEOLDOS device will not deploy the booms in isolation. Whilst some antenna applications are envisioned (Angling et al., 2013), it is primarily intended that the booms will extend an aerobrake membrane. Therefore the experiments are repeated with representative (e.g. Shmuel et al., 2012) membranes of 12 μm metallised polyester being extended from the stowage chambers. A typical deployment is shown in Fig. 6, where the weight of the booms was supported by a low-friction table to maintain linear deployment of the booms.

The results of the second round of testing are presented in Fig. 7. In these cases neither hub attains a steady-state deployment as the increasing amount of energy required to unfold a growing area of membrane begins to exceed the power delivered by the tape-springs, although the longer transient at the conclusion of deployments from petal-hubs is maintained. It is also noticeable that the 708 mm deployment from the traditional hub lasted slightly longer than expected, perhaps due to weaknesses in the hub/boom connection. However, as Fig. 8 goes on to show, the petal-hub generally offers a highly-repeatable and predictable deployment performance even with the membrane attached.

2.1.3. Sail-casting doors

As the series of high-speed images in Fig. 9 show, the booms angle slightly in response to the guide bearings during the early stages of deployment. This is exploited to rotate and separate the sail-casting doors. It is also worth noting that the high-speed footage indicates that the deployment-end vibration suggested in the literature (Adeli, 2010) is a real effect, and so wave-springs are introduced at the boom-door interface to absorb this motion. These springs can also absorb some creep of the booms that may be expected due to thermal and thermal cycling effects during the dormant period, helping to ensure that the device does not begin to open prematurely.

Some interesting points in Fig. 9 are illustrated at points A, B and C. Point A is an LED that illuminates when the solenoid is fired to release the hub, the appearance of the light allowing a time datum to be set for the video footage, while point B indicates one of the lugs that secure the doors prior to deployment. C is the rotation rate sensor, which is connected to the hub inside the module.

The entire sequence shown takes less than one-tenth of a second, and when considered with the reliability and repeatability illustrated in Fig. 8, we conclude that the petal-hub system is an attractive and scalable concept for tape-spring deployment purposes.

2.2. Enabling concept #2: folding and deployment optimisation

The membrane must be unfolded from AEOLDOS by the action of the tape-springs during deployment, and the approach adopted is to use the inside of the sail-casting doors as tow-points for the two outboard corners of each of the four isosceles-triangular sub-sails while the third apex remains affixed to the AEOLDOS module itself.

Naturally the sail must be folded such that, (i), the most efficient use is made of the stowage chambers and that, (ii), the action of the sail-casting doors can open all the folds in the sequence required for full deployment. As the stowage chambers have an unusual form, namely the isosceles-trapezoidal prisms already suggested in Fig. 4, a MATLAB script is written to design the appropriate fold pattern with respect to some global parameters. The unfolding process is then examined by a validated numerical model.

The folding scheme used is an adaption of the frog-leg pattern described in the literature (Dalla Vedova et al., 2011), but with a modification such that the secondary folds are spaced to produce an angled sail membrane

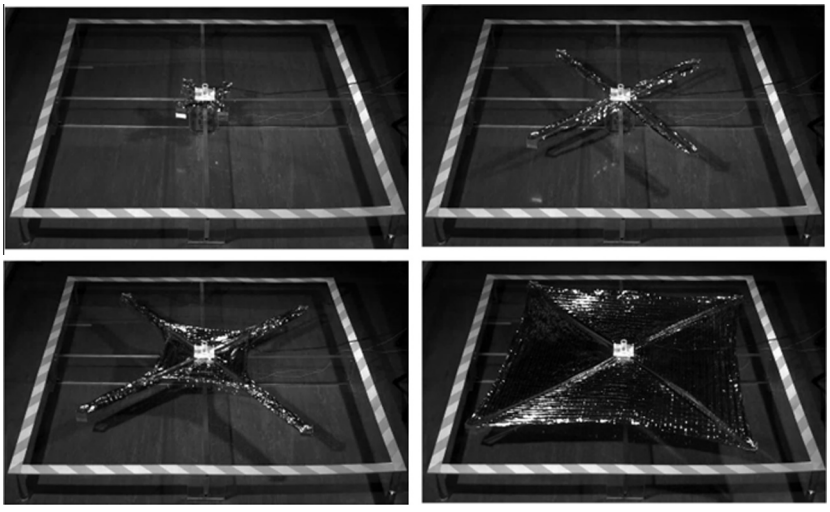

Fig. 6. The deployment of an 867 mm boom (1.5 m^2) system on a Perspex table. The high-speed images are taken at deployment plus 0.08 s, 0.17 s, 0.22 s and 0.32 s.

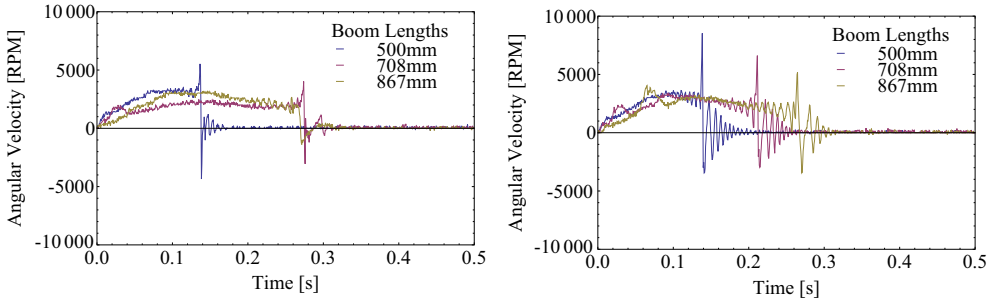

Fig. 7. The behaviour of a traditional hub (left) and a petal-hub (right), with membranes attached, and boom lengths of 500 mm, 708 mm and 867 mm.

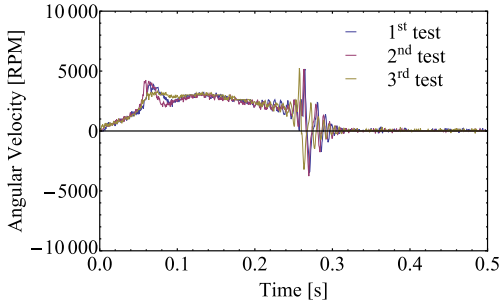

Fig. 8. Three consecutive deployments of 867 mm booms from an AEOLDOS device with membranes attached. The features at 0.25 s are the post-deployment oscillations.

package that fits precisely into the isosceles-trapezoidal storage volume. If this is achieved correctly, a sail with corner angle θ will yield a sail membrane package with corner angles θ_p, where $\theta = \theta_p$. This pattern, which we term the 'angled frog-leg', is shown in Fig. 10.

2.2.1. Preliminary folding

The folding process begins by first folding each sub-sail, using equally-spaced preliminary folds, into a Preliminary Folded Strip (PFS). Transverse secondary folds are then applied (see below) to produce the sail membrane package, with the folds distributed such that the sail membrane package adopts the desired shape in which $\theta = \theta_p$. This process is, however, complicated by the fact that the PFS is much thicker at the centre than at the ends.

Nonetheless, the thickness of the strip may be calculated by adding up the number of layers in the PFS and then multiplying by the membrane thickness. Assuming that the preliminary folds are equally spaced w_p apart such that the width of the PFS is equal to the height of the chamber, the number of layers and hence the thickness of the strip will increase in a predictable, stepwise manner from the ends towards the centre with a new layer appearing every $w_p\cot\theta$ along the path.

2.2.2. Secondary folding

Rather than affixing the very apex of the sub-sail to the rear wall of the stowage chamber, an attachment baseline is used. This baseline is the same length as the back of the stowage chamber, and the first secondary folds are placed at either end of the baseline at a distance of $2w_{s1}$ apart.

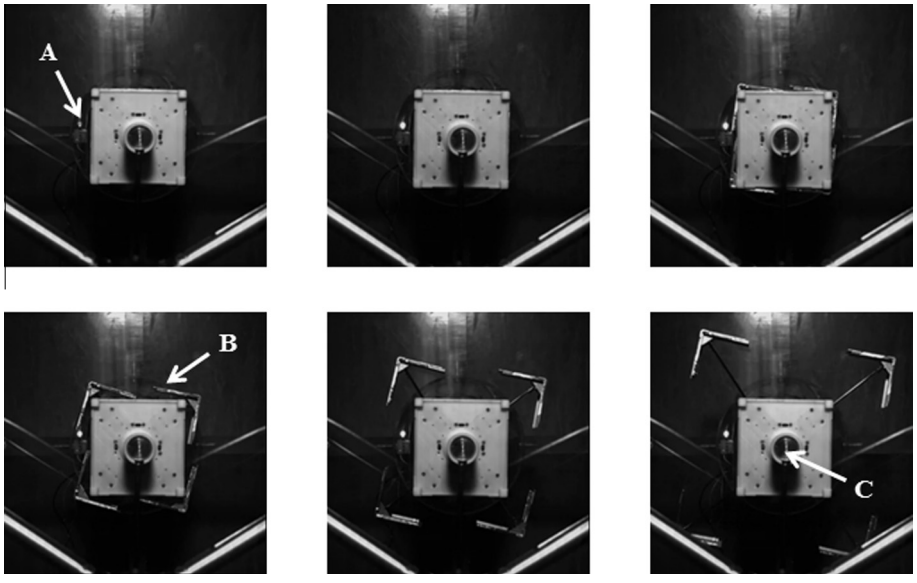

Fig. 9. The sail-casting doors rotate and separate before moving outwards over the course of less than one-tenth of a second. In service, they would also extract the aerobrake membrane. Points A, B and C are described in the text.

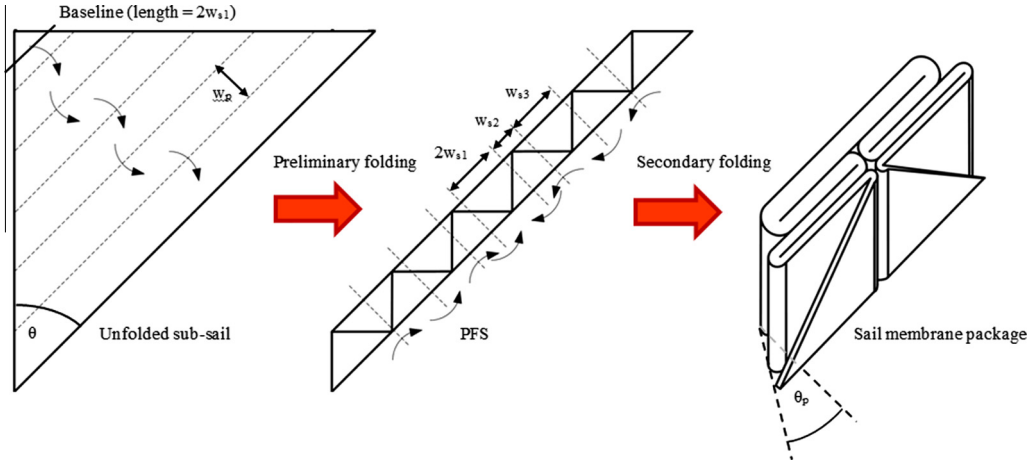

Fig. 10. The angled frog-leg folding pattern adopted for each sub-sail of the AEOLDOS module.

The second secondary folds are placed after a distance of w_{s2}, the third w_{s3} after that, and so on.

As w_{s1} is set by the baseline, the spacing of the following folds all build on this condition. w_{s2} is set equal to w_{s1} to bring each leg back to the centre of the chamber, but w_{s3} is marginally longer because the chamber widens as one moves away from the rear wall. The distance one has moved away from the rear wall is equal to the total running folded thickness, which can be calculated by considering the number of layers and the thickness of the membrane, while the expansion of the chamber at this displacement from the rear wall is a simple function of the angle θ.

These processes are written into a MATLAB script, along with two minor improvements. Firstly, the script tracks the position of the secondary folds, as on every other turn it is possible that the profile of the newly-folded layer can interleave with the layer below to produce a one-membrane thickness reduction; and secondly, the code maintains a full membrane-thickness of clearance at the walls of the stowage chamber to accommodate the fold radii. Some typical results at different values of the parameters A, n and T, which represent aerobrake area, number of sub-sails and membrane thickness, appear in Fig. 11. Plots such as these may then be used as practical folding templates.

Sail membrane packages based on total sail areas of 1, 1.5 and 3 m^2 are created based on the algorithm previously described and their volume compared to the predicted values. The package representing one sub-sail of a 3 m^2, 12 μm aluminised polyester aerobrake, along with a thin-walled cartridge designed to fit into the stowage chamber for ease of membrane installation and removal, is shown in Fig. 12. Overall the three folded sail membrane packages trialled are, on average, 11% larger in volume than their theoretical predictions. However, this value should be treated with caution due to the sensitivity of the calculation to measurements taken across the slightly uneven packages.

2.2.3. Deployment

To unfold without stalling the secondary folds must release before the preliminary folds. As Fig. 6 suggests, the movement of the sail-casting doors first causes the secondary folds to open from outboard to inboard, and then the preliminary folds open from inboard to outboard. This is intuitively consistent with the shortest possible fold-length always opening to satisfy the ongoing expansion, as the number of layers associated with each secondary crease line increases towards the apex while the last preliminary fold lines to open are the longest ones towards the outboard edge.

To provide scope for the examination of this behaviour in more detail, the commercial package LS-Dyna is used to model a deployment process. Using a simplified sub-sail extracted by boundary conditions applied at the two outboard corners, and with only four preliminary and four secondary folds, the results portrayed in Fig. 13 suggest that the secondary-preliminary unfolding pattern can be resolved by this package.

Expansion of the model to replicate a full sub-sail causes more and more self-interactions during the deployment, which ultimately destabilise the model behaviour. However, if self-penetrations are permitted, Fig. 14 illustrates that it is still possible to obtain behaviour that is reasonably predictive of observed events. Furthermore, as the model is run with no atmospheric or pressure perturbations, this process builds confidence that similar successful deployments may be achieved in the space environment. The combination of high packaging efficiency and robust deployment performance is considered to make the angled frog-leg a very attractive fold architecture for the AEOLDOS module.

2.3. Enabling concept #3: release

AEOLDOS deploys by releasing stored strain. Such mechanisms are often triggered by a pin-puller or pyro-cutter, but mass and certification issues may make these unattractive to CubeSat operators. Accordingly alternative burn-through release devices are often employed instead, where Nichrome wire (Puig-Suari et al., 2001) or resistors (Senatore et al., 2009) are used to burn through Dyneema

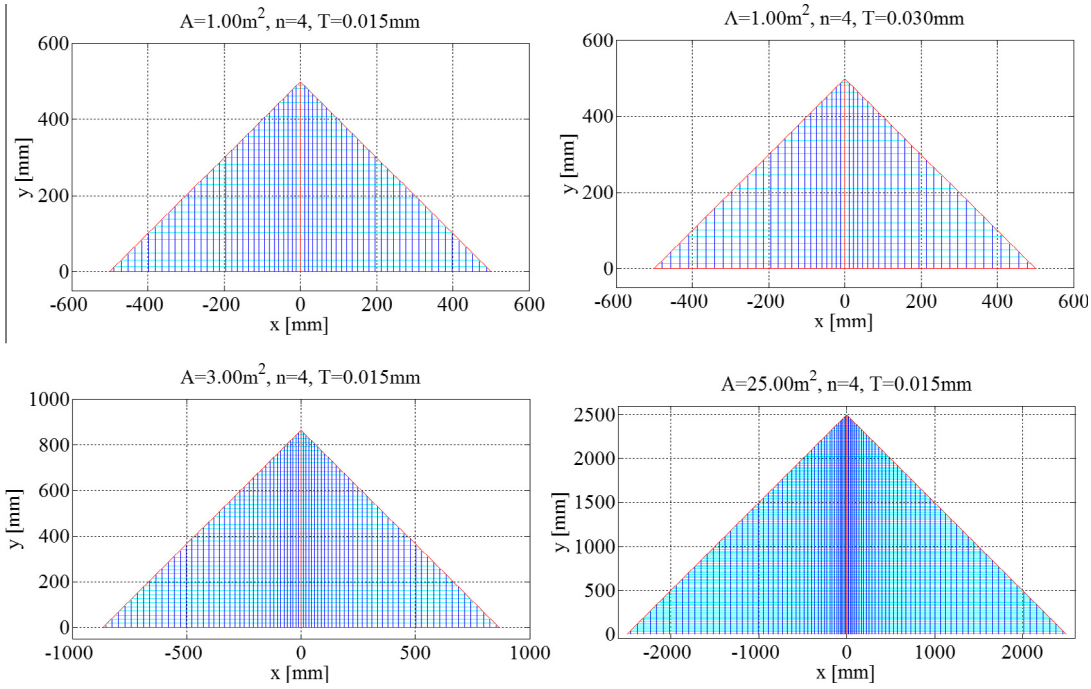

Fig. 11. Typical fold patterns for various sub-sail parameters. The rear area of the cartridge is assumed to be 21 mm ($2w_{s1}$) × 18 mm, as defined by AEOLDOS' volume requirements.

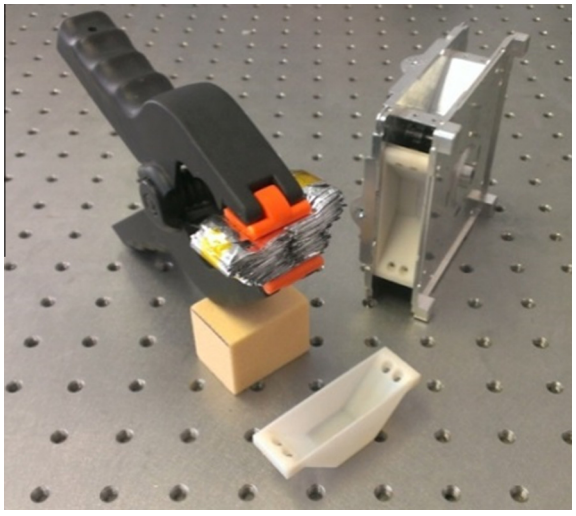

Fig. 12. A sail membrane package representing one sub-sail of a 3 m^2 aerobrake is folded and ready for the cartridge below. The cartridges will slot into stowage chambers on AEOLDOS.

(Fernandez et al., 2012), Vectran (Thurn et al., 2012) or similar cord.

However, it is often the case that the cord and heating element are held in contact before deployment. This can require a complicated array of springs, bearings and linkages (Thurn et al., 2012), and often reacts a significant load into a thermal element that must, almost by definition, be relatively thin. To eliminate this stress a simple cord-cutting module is proposed for AEOLDOS. This cutter will use a thermally-activated Shape-Memory Alloy (SMA) element as the heating element and take advantage of the shape-changing behaviour such that the cord does not touch the element until the cut is desired.

To achieve this behaviour, the SMA element is straight-annealed and placed in the cord-cutting module with the free ends passing through ports, thus deforming elastically into a C-shape. The C-shape may then be further deformed, apparently plastically, to approximate a figure-eight shape with up to 8% strain being recoverable (Poncet, 2000) before the cord is fed through the centre, as shown in Fig. 15. When a voltage is applied to the element ohmic heating triggers a martensite-austenite phase

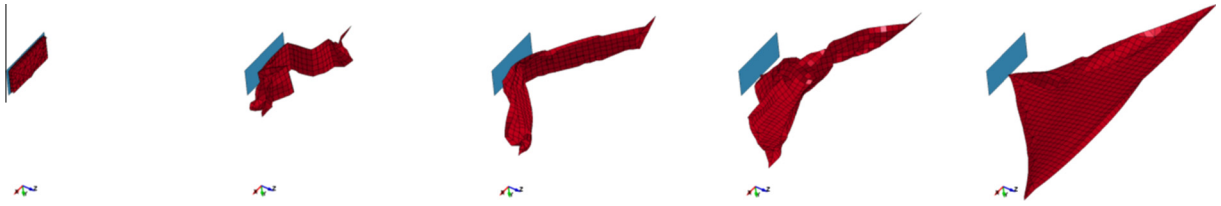

Fig. 13. With four preliminary and four secondary folds, LS-Dyna can resolve the main features of the unfolding process recorded in Fig. 5.

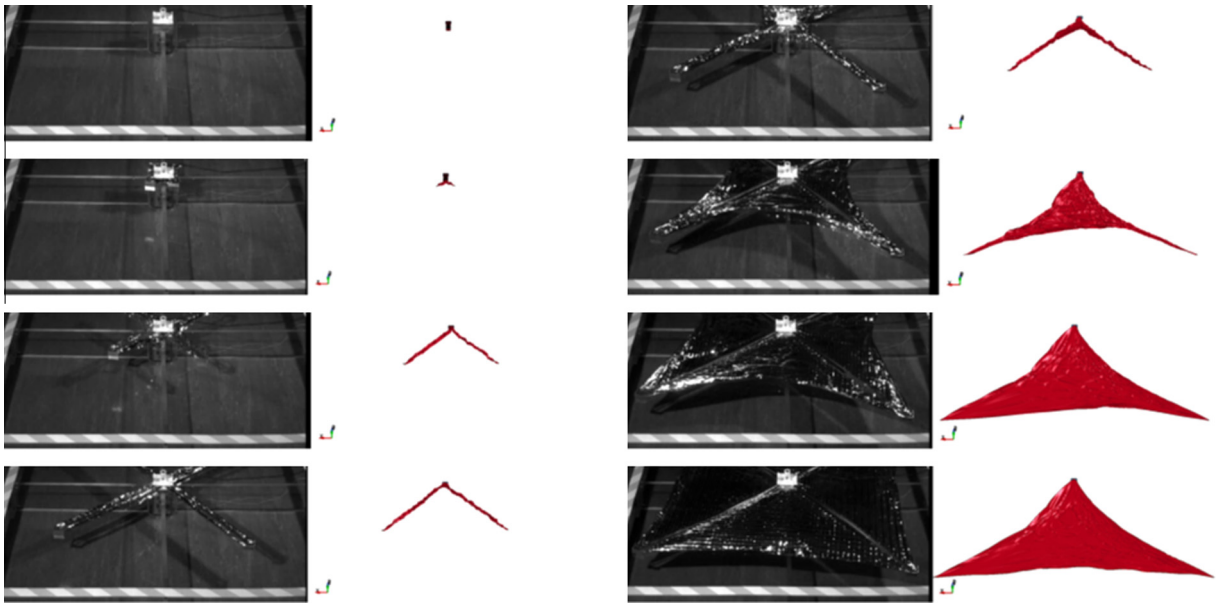

Fig. 14. A highly-simplified model of the sub-sail, with self-penetrations permitted, still resolves the fundamental behaviour of the deployment process.

change, tending to recover the annealed shape and shearing the cord between two sections of hot SMA. The operating temperature may be tailored according to the melting temperature of the intended cord, and operations may be monitored through the electrical characteristics of the element itself (Abel et al., 2004).

The behaviour is revealed in thermal images, as shown in Fig. 16. During the operation shown in these images, a 0.38 mm Dyneema cord was sheared within two seconds of the current being applied.

The effectiveness of the cord-cutting module is a function of the amount of current passed through the wire. An experimental setup in which 0.38 mm Dyneema cord is passed through a cutting module is used to determine the time to cut the cord with different electrical currents, with the time being measured between a rising signal at the application of the current and a falling signal when a force transducer mounted above the module ceases to register a 4 N mass suspended through it. Using a LT (low temperature) Flexinol alloy with a transition temperature of 70 °C and diameter of 0.38 mm, and a HT (high temperature) Flexinol alloy with a 90 °C transition temperature and 0.51 mm diameter, the results presented in Fig. 17 are obtained in laboratory conditions.

It is apparent that, beyond a certain threshold, diminishing returns are obtained for additional current in terms of cutting time. Nonetheless, the cutting times observed are reasonable and performance in vacuum may be improved still further (Thurn et al., 2012). It can therefore considered likely that an effective and robust release of the stored strain may be achieved within realistic current and time-to-cut limitations. One caution, however, is that excessive current may heat the wire to above its annealing temperature (Pelton et al., 2004), with permanent changes to the microstructure and consequent effects on the repeatability of the device.

3. Performance of the AEOLDOS system

The AEOLDOS module incorporates three enabling technologies; the petal hub, the angled frog-leg fold pattern, and the cord-cutter; to produce a module of 0.4U with a mass of 372 g that can deploy aerobrake membranes of up to 3 m^2 as standard. This module is fully compatible

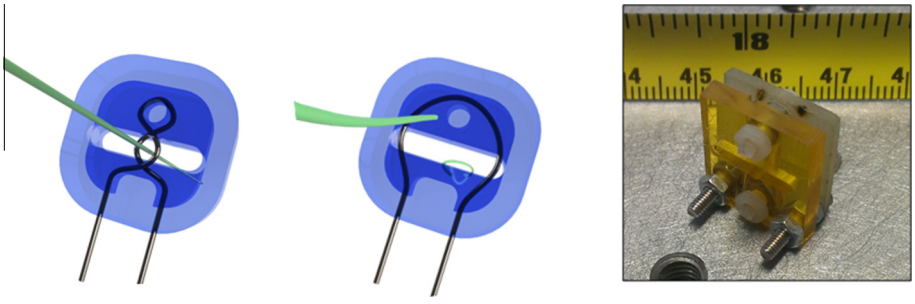

Fig. 15. The cord passes through the figure-eight of martensitic material (left), but when a voltage is applied ohmic heating forces an austenitic phase change and shears the cord between two sections of the element (centre). At right, a functional prototype of the cord-cutting module.

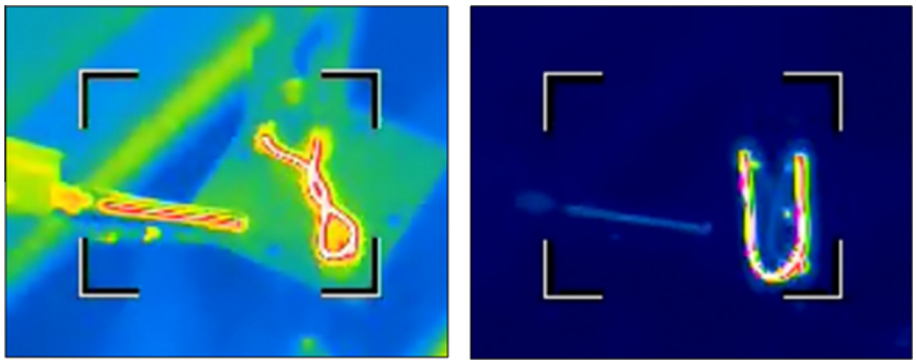

Fig. 16. The deformation of a straight-annealed SMA wire in a prototype cord-cutting module. Warm colours represent higher temperatures.

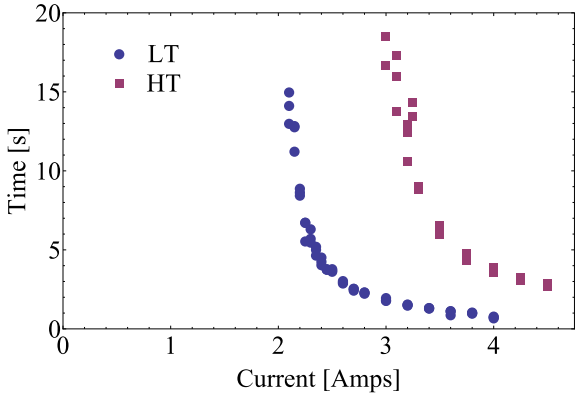

Fig. 17. Time taken to cut 0.38 mm Dyneema cord in a prototype cord-cutting module, with two different SMA elements. The load on the cord is 4 N and the cord-cutting module has a mass of less than one gram.

with the CubeSat architecture, can host solar cells on the top surface, and incorporates cable pass-throughs for crossing services.

The deorbit performance of the AEOLDOS module will depend on the orbital parameters and atmospheric conditions between deployment and final re-entry, and every mission will require a dedicated analysis. However, there is every reason to expect that deorbit will be hastened by a considerable degree if an AEOLDOS-like device is employed (Roberts and Harkness, 2007), (Lappas et al., 2011) and the change in ballistic coefficient that the device can produce, which may be up to several hundred-fold, is a useful starting point for individual lifetime calculations.

As an exemplar of this, consider the work of (Fernandez et al., 2013). This suggests that the 25-year 'ceiling' may be elevated from 650 km for a 'typical satellite' to 800 km in the case of a 100 kg satellite with a 10 m^2 drag sail. Based on this work AEOLDOS, which is designed to deploy a 3 m^2 drag sail from a ~3 kg spacecraft, would produce a ballistic coefficient ten times lower than the one put forward in the (Fernandez et al., 2013) scenario. This provides confidence that the orbits made available by AEOLDOS-like devices extend well over 100 km above the current effective 25-year limit.

4. Conclusion

A number of novel technologies have been described and characterised. The petal-hub has been shown to provide highly-repeatable deployment of the tape-springs into a radial shape, which may be exploited by the use of the angled frog-leg pattern. The fold pattern has been shown to open sequentially, minimising the risks for fouling and stalling during deployment. Finally, deployment may be triggered by a cord-cutting module that has been shown to offer highly-predictable burn-though times at realistic electrical current values.

Taken together, these technologies enable a CubeSat-compatible module that has the capability to significantly reduce the decay time of small satellites and which may be exploited for other purposes such as antenna and solar sailing applications.

This device, with some modifications to facilitate compliance with standards such as ECSS, is now offered as a commercial product and may be tailored, in terms of deployed area, to match customer requirements within the broad parameter space outlined above.

Acknowledgement

This work was supported by the Engineering and Physical Sciences Research Council [Grant No. EP/K503514/1]

References

Abel, E., Luo, H., Pridham, M., et al., 2004. Issues concerning the measurement of transformation temperatures of NiTi alloys. Smart Mater. Struct. 13 (5).

Adeli, N. 2010. Deployment system for the CubeSail nano-solar sail mission. In: 24th ASU/AIAA Conference on Small Satellites, Logan, USA.

Angling, M., Harkness, P., McRobb, M., et al., 2013. The wideband ionospheric sounder CubeSat experiment. In: The International Beacon Satellite Symposium. Bath, UK.

Banik, J., Murphey, T. 2007. Synchronous deployed solar sail subsystem design concept. In: AIAA, pp. 2007–1837.

Ceriotti, M., Harkness, P., McRobb, M., 2013. Variable-geometry solar sailing: the possibilities of the Quasi-Rhombic Pyramid. In: International Symposium on Solar Sailing. Glasgow, UK.

Dalla Vedova, F., Henrion, H., Leipold, M., et al., 2011. The solar sail materials (SSM) project – status of activities. Adv. Space Res. 48, 1922–1926.

Fernandez, J., Lappas, V., Daton-Lovett, A. 2012. The completely stripped solar sail concept. In: 53rd AIAA/ASME/ASCE/AHS/ASC Structures, Structural Dynamics and Materials Conference, Honolulu, Hawaii, USA.

Fernandez, J., Schenck, M., Prassinos, G., Lappas, V., Erb, S.O. 2013. Deployment mechanisms of a gossamer satellite deorbiter. In: 15th European Space Mechanisms and Tribology Symposium, Noordwijk, The Netherlands.

Freeland, R.E. 1998. Inflatable deployable space structures technology summary. In: IAF-98-I.5.01, 49th International Astronautical, Congress, Melbourne, Australia.

Jeon, S. Murphey, T. 2011. Design and analysis of a meter-class CubeSat boom with a motor-less deployment by bi-stable tape springs. In: 52nd AIAA/ASME/ACSE/AHS/ASC Structures, Structural Dynamics and Materials Conference, Denver, USA.

Johnson, L., Whorton, M., Heaton, A., et al., 2011. Nano-Sail-D: a solar sail demonstration mission. Acta Astronaut. 68 (5–6).

King-Hele, D., 1987. Satellite Orbits in an Atmosphere. Blackie, ISBN 0-216-92252-6.

Kuwahara, T., Tomioka, Y., Tanabe, Y., et al., 2011. Development status of micro-satellite de-orbit mechanisms for active prevention and reduction of space debris. In: The 3rd Nano-Satellite Symposium, Kitakyushu International Conference Center, Japan.

Lappas, V., Adeli, N., Visagie, L., et al., 2011. CubeSail: a low cost CubeSat based solar sail demonstration mission. Adv. Space Res. 48 (11).

Lee, S., 2006. Co-ordination of multiple CubeSats on the Dnepr launch vehicle (M.Sc. thesis), California Polytechnic State University.

Lücking, C., Colombo, C., McInnes, C., 2011. A passive de-orbiting strategy for high altitude CubeSat missions using a deployable reflective balloon. In: 8th IAA Symposium on Small Satellites, Berlin, Germany.

Pardini, C., Hanada, T., Krisko, P., 2009. Benefits and risks of using electrodynamic tethers to de-orbit spacecraft. Acta Astronaut. 64 (5–6).

Pelton, A.R., Duerig, T.W., Stockel, D., 2004. A guide to shape memory and superelasticity in Nitinol medical devices. Minimal. Invasive Ther. Allied Technol. 13 (4).

Poncet, P., 2000. Nitinol medical device design considerations. Strain 2 (6).

Puig-Suari, J., Turner, C., Ahlgren, W., 2001. Development of the standard CubeSat deployer and a CubeSat class picosatellite. IEEE Proceedings, vol. 1.

Roberts, P., 2004. Drag sail dynamics for end of life deorbit. In: AAS 04–209, 14th AAS/AIAA Space Flight Mechanics Conference, Maui, Hawaii, USA.

Roberts, P., Harkness, P., 2007. Drag sail for end-of-life disposal from low earth orbit. J. Spacecraft Rockets 44 (6).

Seffen, K., Pellegrino, S., 1999. Deployment dynamics of tape-springs. Proc. R. Soc. London, A 455, 1003–1048.

Senatore, P., Klesh, A., Zurbuchen, T., et al., 2009. Concept, design, and prototyping of XSAS: a high power extendable solar array for CubeSat applications. In: 40th Aerospace Mechanisms Symposium, NASA Kennedy Space Center, USA.

Shmuel, B., Hiemstra, J., Tarantini, V., et al., 2012. The canadian advanced nanospace eXperiment (CanX-7) demonstration mission: deorbiting nano-and microspacecraft. In: SSC12-I-9, 26th Annual AIAA/USI Conference on Small Satellites, Logan, Utah, USA.

Thurn, A., Huynh, S., Koss, S., et al., 2012. A Nichrome burn wire release mechanism for CubeSats. In: 41st Aerospace Mechanisms Symposium, Pasadena, California, USA.